Supplement of Atmos. Chem. Phys., 21, 4403–4430, 2021
https://doi.org/10.5194/acp-21-4403-2021-supplement

Atmospheric Chemistry and Physics Open Access

Supplement of

Improving the sectional Model for Simulating Aerosol Interactions and Chemistry (MOSAIC) aerosols of the Weather Research and Forecasting-Chemistry (WRF-Chem) model with the revised Gridpoint Statistical Interpolation system and multi-wavelength aerosol optical measurements: the dust aerosol observation campaign at Kashi, near the Taklimakan Desert, northwestern China

Wenyuan Chang et al.

Correspondence to: Wenyuan Chang (changwy@mail.iap.ac.cn) and Zhengqiang Li (lizq@radi.ac.cn)

Table S1. Real and imaginary parts of complex refractive indexes of aerosol chemical compositions and water

(nm)	440	450	470	520	525	550	635	660	675	870	1020
						Sulfate, Nitrate, Ammonium (Toon et al., 1976)					
Real	1.54	1.54	1.54	1.535	1.53	1.53	1.53	1.525	1.525	1.52	1.52
Imag						0					
						OC (Chen and Bond, 2010)					
Real						1.55					
Imag						0.001					
						BC (Bond and Berstrom, 2006)					
Real						1.95					
Imag						0.79					
						Chlorine, Sodium (Toon et al., 1976)					
Real	1.56	1.56	1.56	1.55	1.55	1.55	1.55	1.54	1.54	1.53	1.53
Imag						0					
						OIN, dust (Cheng et al., 2006; Zhao et al., 2010)					
Real						1.53					
Imag	0.003	0.003	0.003	0.0025	0.0025	0.002	0.0015	0.0015	0.0015	0.001	0.001
						H_2O					
Real	1.337	1.337	1.337	1.337	1.335	1.335	1.335	1.335	1.332	1.33	1.328
Imag						0					

† The refractive indexes that are constant across the wavelengths are only written at 550 nm for clarity.

Table S2. Aerosol density (unit: g cm^{-3}; Barnard et al., 2010)

SO4	NO3	NH4	CL	NA	OC	BC	OIN	H2O
1.8	1.8	1.8	2.2	2.2	1.4	1.8	2.6	1.0

References

Barnard, J. C., Fast, J. D., Paredes-Miranda, G., Arnott, W. P., and Laskin, A.: Technical Note: Evaluation of the WRF-Chem "Aerosol Chemical to Aerosol Optical Properties" Module using data from the MILAGRO campaign, Atmos. Chem. Phys., 19, 7325-7340, doi:10.5194/acp-10-7325-2010, 2010.

Bond, T. C., and Bergstrom, R. W.: Light absorption by carbonaceous particles: an investigative review, Aerosol Sci. Tech., 40, 27-67, doi:10.1080/02786820500421521, 2006.

Chen, Y., and Bond, T. C.: Light absorption by organic carbon from wood combustion, Atmos. Chem. Phys., 10, 1773-1787, doi:10.5194/acp-10-1773-2010, 2010.

Cheng, T., Wang, H., Xu, Y., Li, H., and Tian, L.: Climatology of aerosol optical properties in northern China, Atmos. Environ., 40, 1495-1509, doi:10.1016/j.atmosenv.2005.10.047, 2006.

Toon, O. B., Pollack, J. B., and Khare, B. N.: The optical constants of several atmospheric aerosol species: ammonium sulfate, aluminum oxide, and sodium chloride, J. Geophys. Res., 81, 33, doi:10.1029/JC081i033p05733, 1976.

Zhao, C., Liu, X., Leung, L. R., Johnson, B., McFarlane, S. A., Gustafson Jr., W. I., Fast, J. D., and Easter, R.: The spatial distribution of mineral dust and its shortwave radiative forcing over North Africa: modeling sensitivities to dust emissions and aerosol size treatments, Atmos. Chem. Phys., 10, 8821-8838, doi:10.5194/acp-10-8821-2010, 2010.

Table S3. Mean biases, correlation coefficients (R) of $PM_{2.5}$ and PM_{10} and the $PM_{2.5}/PM_{10}$ ratios in DA_PMx in the model background and the analyses at Kashi in April 2019 as scaling the background error of the fourth size-bin OIN (oin_a04).

	$PM_{2.5}$ (μg m^{-3})		PM_{10} (μg m^{-3})		$PM_{2.5}/PM_{10}$
	Mean Bias	R	Mean Bias	R	
Observation	91.0		323.2		0.28
Background	–15.7	0.28	–132.5	0.24	0.39
DA Analysis					
1.0×oin_a04	–1.7	0.89	6.1	0.99	0.27
0.9×oin_a04	2.46	0.91	6.76	0.99	0.28
0.8×oin_a04	3.29	0.94	4.09	0.98	0.29
0.7×oin_a04	5.17	0.95	-1.92	0.99	0.30
0.6×oin_a04	5.94	0.97	-4.29	0.98	0.31
0.5×oin_a04	6.63	0.97	-12.39	0.98	0.32
0.4×oin_a04	6.62	0.98	-18.47	0.98	0.33
0.3×oin_a04	5.92	0.98	-26.4	0.97	0.33

Table S4a. $PM_{2.5}$, PM_{10}, and the aerosol number concentrations in the second (num_a02) and the fourth (num_a04) size bin at Kashi on 1200UTC April 9, 2019, when individually assimilating aerosol absorption coefficient (DA_Eabs) with the different imaginary parts of the dust complex refractive index at 470, 520, and 660 nm.

			$PM_{2.5}$ ($\mu g/m^3$)	PM_{10} ($\mu g/m^3$)	num_a02 (#/kg)	num_a04 (#/kg)
Observation			157	617		
Imaginary part of dust refractive index						
470nm	520nm	660nm				
0	0	0	698	1987	71222226176	7298349
0.001	0.001	0.001	559	1771	5019896320	6861575
0.008	0.008	0.008	306	860	2681975552	3133878
0.01	0.01	0.01	275	742	2398040064	2647442
0.02	0.02	0.02	230	532	2182263040	1710307

Table S4b. The same to Table S4a but for Eabs, Eabs/PM_{10}, Esca, and SSAsrf†.

			660 nm Eabs ($M\ m^{-1}$)	660nm Eabs/PM_{10} ($M\ m^{-1}\ \mu g\ m^{-3}$)	520 nm Eabs ($M\ m^{-1}$)	525 nm Esca ($M\ m^{-1}$)	SSAsrf
Observation			64.4	0.104	90.8	436.8	0.83
Imaginary part of dust refractive index							
470nm	520nm	660nm					
0	0	0	92.5	0.047	144.6	1475.0	0.91
0.001	0.001	0.001	74.5	0.042	118.1	1163.8	0.91
0.008	0.008	0.008	32.5	0.038	52.7	603.1	0.89
0.01	0.01	0.01	28.7	0.039	45.4	532.3	0.92
0.02	0.02	0.02	23.8	0.045	37.6	436.3	0.92

† SSAsrf=Esca525/(Esca525+Eabs520)

Table S5. Analyses of DA_Eabs with different scaling factors for the background errors (bc_a0x) of black carbon at Kashi in April 2019. The underlined number in bold denotes the monthly mean value that is not significantly different from the observation, and the dashed line denotes an insignificant correlation. Both the statistical tests of the mean difference and correlation are conducted at the significance level of 0.05.

DA experiment	$PM_{2.5}$ ($\mu g\ m^{-3}$)	PM_{10} ($\mu g\ m^{-3}$)	870 nm AOD	635nm Esca (Mm^{-1})	660nm Eabs (Mm^{-1})	SSAsrf
Observation	91.0	323.2	0.66	231.5	47.4	0.78
Background	**72.2** (0.29)	190.7 (0.24)	0.24 (0.60)	123.3 (0.36)	12.9 (0.34)	0.86
1×bc_a0x (DA_Eabs)	298.8 (0.36)	1281 (0.34)	1.73 (----)	612.2 (0.54)	**40.0** (0.98)	0.90
2×bc_a0x	244.3 (0.42)	1020 (0.36)	1.46 (0.33)	509.8 (0.55)	**44.3** (1.00)	0.88
3×bc_a0x	209.0 (0.45)	844.1 (0.40)	1.20 (0.36)	425.7 (0.58)	**46.4** (0.98)	0.86
4×bc_a0x	180.3 (0.50)	714.7 (0.46)	1.00 (0.40)	362.0 (0.57)	**48.3** (0.95)	0.84
5×bc_a0x	155.3 (0.48)	599.4 (0.41)	**0.82** (0.40)	306.3 (0.51)	**49.8** (0.93)	0.81
6×bc_a0x	138.2 (0.43)	526.8 (0.43)	0.71 (0.39)	**271.2** (0.49)	**51.8** (0.93)	0.79
7×bc_a0x	**122.4** (0.45)	**463.7** (0.42)	**0.61** (0.43)	**239.4** (0.49)	**53.7** (0.92)	0.78
8×bc_a0x	**110.6** (0.42)	**402.1** (0.38)	**0.53** (0.39)	**213.9** (0.50)	**55.2** (0.90)	0.75
9×bc_a0x	**100.6** (0.37)	**358.7** (0.41)	0.46 (0.36)	**194.4** (0.47)	**56.2** (0.88)	0.73

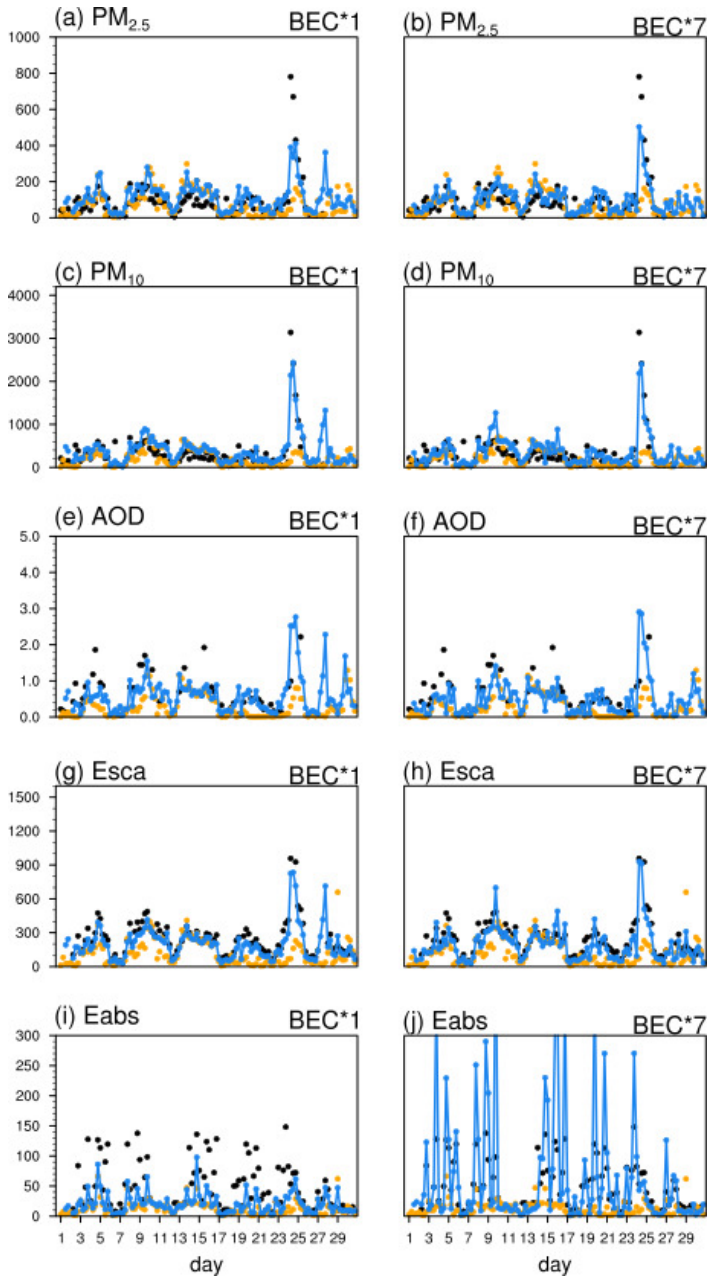

Figure S1. Comparison of (a-b) $PM_{2.5}$ (μg m^{-3}), (c-d) PM_{10} (μg m^{-3}), (e-f) 870 nm AOD, (g-h) 635 nm aerosol scattering coefficient (Esca, Mm^{-1}), and (i-j) 660 nm aerosol absorption coefficient (Eabs, Mm^{-1}) in the observation (black solid point), the background simulation (orange solid point), and the DA analyses (blue line) when assimilating the aerosol scattering and absorption coefficients with the original background error of BC (BEC*1, left column, DA_Esca_Eabs) and the BEC enlarged by a factor of 7 (BEC*7, right column, DA_Esca_Eabs_BC*7) at Kashi in April 2019.